Optical properties of Mn in regrown GaN-based epitaxial layers

Feng-Wen Huang,[1] Jinn-Kong Sheu,[1,2,*] Shang-Ju Tu,[1] Po-Cheng Chen,[1] Yu-Hsiang Yeh,[1] Ming-Lun Lee,[3] Wei-Chih Lai,[1,2] Wen-Che Tsai,[4] and Wen-Hao Chang[4]

[1]*Department of Photonics & Advanced Optoelectronic Technology Center, National Cheng Kung University, Tainan City 70101, Taiwan*
[2]*Center for Micro/Nano Science and Technology, National Cheng Kung University, Tainan City 70101, Taiwan*
[3]*Department of Electro-Optical Engineering, Southern Taiwan University, Tainan County 71001, Taiwan*
[4]*Department of Electrophysics, National Chiao Tung University, Hsinchu, 300 Taiwan*
**jksheu@mail.ncku.edu.tw*

Abstract: The memory effect and redistribution of manganese (Mn) into subsequently regrown GaN-based epitaxial layers by metalorganic chemical vapor deposition were revealed. Low-temperature up-converted photoluminescence (UPL) and the secondary ion mass spectrometry were performed on GaN-based epitaxial samples with and without Mn doping to study the effect of residual Mn on optical property. UPL emission, which originated from residual Mn doping in regrown InGaN quantum wells (QWs) because of the memory effect of the reactor, could be eliminated in an air-exposed and H_2-baking manner prior to the regrowth of the QWs. Considerable residual Mn background level and slow decay rate of Mn concentration tail were also observed in the regrown epitaxial layers, which could be attributed to the memory effect or surface segregation and diffusion from the Mn-doped underlying layer during regrowth in the Mn-free reactor.

OCIS codes: (160.6000) Semiconductor materials; (230.0250) Optoelectronics; (350.6050) Solar energy.

References and links

1. S. J. Pearton, C. R. Abernathy, D. P. Norton, A. F. Hebard, Y. D. Park, L. A. Boatner, and J. D. Budai, "Advances in wide bandgap materials for semiconductor spintronics," Mater. Sci. Eng. Rep. **40**(4), 137–168 (2003).
2. D. D. Awschalom and M. E. Flatte, "Challenges for semiconductor spintronics," Nat. Phys. **3**(3), 153–159 (2007).
3. A. Luque and A. Martí, "Increasing the efficiency of ideal solar cells by photon induced transitions at intermediate levels," Phys. Rev. Lett. **78**(26), 5014–5017 (1997).
4. A. Luque and A. Martí, "A metallic intermediate band high efficiency solar cell," Prog. Photovolt. Res. Appl. **9**(2), 73–86 (2001).
5. A. Martí, C. Tablero, E. Antolin, A. Luque, R. P. Campion, S. V. Novikov, and C. T. Foxon, "Potential of Mn doped $In_{1-x}Ga_xN$ for implementing intermediate band solar cells," Sol. Energy Mater. Sol. Cells **93**(5), 641–644 (2009).
6. A. Luque and A. Martí, "Photovoltaics: towards the intermediate band," Nat. Photonics **5**(3), 137–138 (2011).
7. T. Trupke, M. A. Green, and P. Wurfel, "Improving solar cell efficiencies by up-conversion of sub-band-gap light," J. Appl. Phys. **92**(7), 4117–4122 (2002).
8. A. Shalav, B. S. Richards, T. Trupke, K. W. Kramer, and H. U. Gudel, "Application of $NaYF_4:Er^{3+}$ up-converting phosphors for enhanced near-infrared silicon solar cell response," Appl. Phys. Lett. **86**(1), 013505 (2005).
9. T. Trupke, A. Shalav, B. S. Richards, P. Wurfel, and M. A. Green, "Efficiency enhancement of solar cells by luminescent up-conversion of sunlight," Sol. Energy Mater. Sol. Cells **90**(18-19), 3327–3338 (2006).
10. F. W. Huang, J. K. Sheu, M. L. Lee, S. J. Tu, W. C. Lai, W. C. Tsai, and W. H. Chang, "Linear photon up-conversion of 450 meV in InGaN/GaN multiple quantum wells via Mn-doped GaN intermediate band photodetection," Opt. Express **19**(S6 Suppl 6), A1211–A1218 (2011).
11. T. Dietl, H. Ohno, F. Matsukura, J. Cibert, and D. Ferrand, "Zener model description of ferromagnetism in zinc-blende magnetic semiconductors," Science **287**(5455), 1019–1022 (2000).

#164357 - $15.00 USD Received 7 Mar 2012; revised 22 Mar 2012; accepted 22 Mar 2012; published 26 Mar 2012

12. A. M. Mahros, M. O. Luen, A. Emara, S. M. Bedair, E. A. Berkman, N. A. El-Masry, and J. M. Zavada, "Magnetic and magnetotransport properties of (AlGaN/GaN):Mg/(GaMnN) heterostructures at room temperature," Appl. Phys. Lett. **90**(25), 252503 (2007).
13. N. Nepal, M. O. Luen, J. M. Zavada, S. M. Bedair, P. Frajtag, and N. A. El-Masry, "Electric field control of room temperature ferromagnetism in III-N dilute magnetic semiconductor films," Appl. Phys. Lett. **94**(13), 132505 (2009).
14. M. H. Kane, M. Strassburg, A. Asghar, W. E. Fenwick, J. Senawiratne, Q. Song, C. J. Summers, Z. J. Zhang, N. Dietz, and I. T. Ferguson, "Alloying, co-doping, and annealing effects on the magnetic and optical properties of MOCVD-grown $Ga_{1-x}Mn_xN$," Mater. Sci. Eng. B **126**(2-3), 230–235 (2006).
15. M. H. Kane, S. Gupta, W. E. Fenwick, N. Li, E. H. Park, M. Strassburg, and I. T. Ferguson, "Comparative study of Mn and Fe incorporation into GaN by metalorganic chemical vapor deposition," Phys. Status Solidi A **204**(1), 61–71 (2007).
16. I. A. Buyanova, M. Izadifard, L. Storasta, W. M. Chen, J. Kim, F. Ren, G. Thaler, C. R. Abernathy, S. J. Pearton, C. C. Pan, G. T. Chen, J. I. Chyi, and J. M. Zavada, "Optical and electrical characterization of (Ga,Mn)N/InGaN multiquantum well light-emitting diodes," J. Electron. Mater. **33**(5), 467–471 (2004).
17. I. A. Buyanova, M. Izadifard, W. M. Chen, J. Kim, F. Ren, G. Thaler, C. R. Abernathy, S. J. Pearton, C. C. Pan, G. T. Chen, J. I. Chyi, and J. M. Zavada, "On the origin of spin loss in GaMnN/InGaN light-emitting diodes," Appl. Phys. Lett. **84**(14), 2599–2601 (2004).
18. I. A. Buyanova, J. P. Bergman, W. M. Chen, G. Thaler, R. Frazier, C. R. Abernathy, S. J. Pearton, J. Kim, F. Ren, F. V. Kyrychenko, C. J. Stanton, C. C. Pan, G. T. Chen, J. I. Chyi, and J. M. Zavada, "Optical study of spin injection dynamics in InGaN/GaN quantum wells with GaMnN injection layers," J. Vac. Sci. Technol. B **22**(6), 2668–2672 (2004).
19. M. H. Ham, S. Yoon, Y. Park, L. Bian, M. Ramsteiner, and J. M. Myoung, "Electrical spin injection from room-temperature ferromagnetic (Ga, Mn)N in nitride-based spin-polarized light-emitting diodes," J. Phys. Condens. Matter **18**(32), 7703–7708 (2006).
20. S. Hövel, N. C. Gerhardt, M. R. Hofmann, F. Y. Lo, D. Reuter, A. D. Wieck, E. Schuster, W. Keune, H. Wende, O. Petracic, and K. Westerholt, "Electrical detection of photoinduced spins both at room temperature and in remanence," Appl. Phys. Lett. **92**(24), 242102 (2008).
21. R. Farshchi, M. Ramsteiner, J. Herfort, A. Tahraoui, and H. T. Grahn, "Optical communication of spin information between light emitting diodes," Appl. Phys. Lett. **98**(16), 162508 (2011).
22. B. T. Jonker, "Progress toward electrical injection of spin-polarized electrons into semiconductors," Proc. IEEE **91**(5), 727–740 (2003).
23. X. Chen, S. J. Lee, and M. Moskovits, "Modification of the electronic properties of GaN nanowires by Mn doping," Appl. Phys. Lett. **91**(8), 082109 (2007).
24. H. C. Koo, J. H. Kwon, J. Eom, J. Chang, S. H. Han, and M. Johnson, "Control of spin precession in a spin-injected field effect transistor," Science **325**(5947), 1515–1518 (2009).
25. Y. R. Shen, *The Principles of Nonlinear Optics* (Wiley, 1984), and references therein.
26. H. M. Cheong, B. Fluegel, M. C. Hanna, and A. Mascarenhas, "Photoluminescence up-conversion in $GaAs/Al_xGa_{1-x}As$ heterostructures," Phys. Rev. B **58**(8), R4254–R4257 (1998).
27. P. P. Paskov, P. O. Holtz, B. Monemar, J. M. Garcia, W. V. Schoenfeld, and P. M. Petroff, "Photoluminescence up-conversion in InAs/GaAs self-assembled quantum dots," Appl. Phys. Lett. **77**(6), 812–814 (2000).
28. K. J. Russell, I. Appelbaum, H. Temkin, C. H. Perry, V. Narayanamurti, M. P. Hanson, and A. C. Gossard, "Room-temperature electro-optic up-conversion via internal photoemission," Appl. Phys. Lett. **82**(18), 2960–2962 (2003).
29. M. R. Olson, K. J. Russell, V. Narayanamurti, J. M. Olson, and I. Appelbaum, "Linear photon upconversion of 400 meV in an AlGaInP/GaInP quantum well heterostructure to visible light at room temperature," Appl. Phys. Lett. **88**(16), 161108 (2006).
30. N. Kuroda, C. Sasaoka, A. Kimura, A. Usui, and Y. Mochizuki, "Precise control of pn-junction profiles for GaN-based LD structure using GaN substrates with low dislocation densities," J. Cryst. Growth **189–190**, 551–555 (1998).
31. Y. Ohba and A. Hatano, "A study on strong memory effects for Mg doping in GaN metalorganic chemical vapor deposition," J. Cryst. Growth **145**(1-4), 214–218 (1994).
32. H. Xing, D. S. Green, H. Yu, T. Mates, P. Kozodoy, S. Keller, S. P. Denbaars, and U. K. Mishra, "Memory effect and redistribution of Mg into sequentially regrown GaN layer by metalorganic chemical vapor deposition," Jpn. J. Appl. Phys. **42**(Part 1, No. 1), 50–53 (2003).
33. H. Zhao, G. Liu, J. Zhang, J. D. Poplawsky, V. Dierolf, and N. Tansu, "Approaches for high internal quantum efficiency green InGaN light-emitting diodes with large overlap quantum wells," Opt. Express **19**(S4 Suppl 4), A991–A1007 (2011).
34. J. Zhang and N. Tansu, "Improvement in spontaneous emission rates for InGaN quantum wells on ternary InGaN substrate for light-emitting diodes," J. Appl. Phys. **110**(11), 113110 (2011).
35. R. M. Farrell, P. S. Hsu, D. A. Haeger, K. Fujito, S. P. DenBaars, J. S. Speck, and S. Nakamura, "Low-threshold-current-density AlGaN-cladding-free m-plane InGaN/GaN laser diodes," Appl. Phys. Lett. **96**(23), 231113 (2010).

#164357 - $15.00 USD Received 7 Mar 2012; revised 22 Mar 2012; accepted 22 Mar 2012; published 26 Mar 2012

36. R. M. Farrell, D. A. Haeger, P. S. Hsu, K. Fujito, D. F. Feezell, S. P. DenBaars, J. S. Speck, and S. Nakamura, "Determination of internal parameters for AlGaN-cladding-free m-plane InGaN/GaN laser diodes," Appl. Phys. Lett. **99**(17), 171115 (2011).

1. Introduction

Semiconductors doped with manganese (Mn) have potential application in the field of spintronics [1,2] and solar cells [3–10]. Most recent studies on dilute magnetic semiconductor materials have focused on Mn-doped GaN for their potential room-temperature application because of the high Curie temperature in spintronics [11–15], such as in memory devices [13], spin-LEDs [16–19], spin-PDs [20,21], and spin-FETs [22–24]. The intermediate band [3–6] and up-conversion [7–10] design can be used for solar cells because they can maximize the efficiency of single gap solar cells using materials with an electronic band within the conventional semiconductor bandgap. Several types of up-conversion methods have been investigated, including second-harmonic generation [25], two-step two-photon absorption process involving quantum dot states [26,27], internal photoemission from a Schottky contact [28,29], and, recently, photo-electron injection originating from an intermediate band absorption of Mn-doped GaN grown by metalorganic chemical vapor deposition (MOCVD) [10]. Manganese doping control in semiconductors is a crucial technology for spintronics and photovoltaic applications. The interface and junction properties strongly affect the performance of these devices with Mn-doped layers. Thus, structure design and the control of the specific Mn doping profiles of these junction devices are important. The significant diffusion behavior of magnesium dopants in III-nitride semiconductors has been revealed when the dislocation density in the epitaxial films is high [30]. Memory effect and redistribution of Mg in the GaN layer grown by MOCVD have been observed [31,32]. These effects cause dopant profiles with a long tail and the resultant imperfect p-n junctions that degrade the performance of bipolar devices. For Mn doping in III-nitride semiconductors, related studies on the memory effect and redistribution are deficient. Consequently, understanding the Mn incorporation efficiency and the redistribution behavior of Mn-doped GaN-based devices during MOCVD growth is necessary. Our preliminary studies reveal that a high residual Mn background level in GaN-based heterostructures may be caused by the source molecular of Mn sticking to the reactor wall of MOCVD (i.e., memory effect). Furthermore, considerable Mn concentration tail (i.e., slow decay tail) was observed in the unintentionally doped layers of GaN-based heterostructures with Mn-doped layer therein. This phenomenon can be caused by the memory effect, surface segregation, and diffusion of Mn during epitaxial growth. In the current paper, the roles of Mn memory effect, surface segregation, diffusion of Mn in GaN grown by MOCVD were systematically studied.

2. Experiments

All samples used in the current study were grown by MOCVD with a vertical stainless reactor (Veeco D-180). The GaN/sapphire templates were made up of a 30 nm-thick GaN nucleation layer grown at 560 °C and 3 μm-thick unintentionally doped GaN (u-GaN) layer grown at 1060 °C on c-face sapphire substrates. These epitaxial layers are denoted as *u-GaN templates*. Another type of template, which is made up of two additional layers, i.e., a 1.0 μm-thick u-GaN layer grown at 1010 °C and a 0.2 μm-thick Si-doped GaN layer grown at 1040 °C, grown on the *u-GaN templates* is denoted as *n-GaN templates*. The background carrier concentrations of the u-GaN and n-GaN samples were about 1×10^{17} and 1×10^{19} /cm^3, respectively. Denoted as sample A, a 30 nm-thick GaN nucleation layer grown at 560 °C, 3 μm-thick u-GaN layer grown at 1060 °C, 0.2 μm-thick Si-doped GaN layer grown at 1040 °C, 10-pair InGaN/GaN MQW structure grown at 770 °C, and 0.2 μm-thick u-GaN cap layer grown at 950 °C were deposited in sequence deposited on c-face sapphire substrates [Fig. 1(a)]. The In-contents and the thicknesses of the InGaN QWs were about 10% and 2 nm, respectively. Sample B had a layer structure similar to that of sample A, but the InGaN/GaN

#164357 - $15.00 USD Received 7 Mar 2012; revised 22 Mar 2012; accepted 22 Mar 2012; published 26 Mar 2012

MQW structure was regrown on the *n-GaN template*, as shown in Fig. 1(b). Note that the InGaN/GaN MQW structure in sample B was regrown after a Mn-containing growth round and H_2 baking. In the current study, all the Mn-doped GaN-based epitaxial layers used bismethylcyclopentadienyl manganese [$(MeCp)_2Mn$] as the Mn source. The growth temperature, growth pressure of the Mn-doped GaN and flow rate of the Mn source were 1010°C, 100 Torr and 2.84 µmole/min, respectively. As shown in Fig. 1(c), sample C had a layer structure and regrowth procedure similar to that of sample B, but the InGaN/GaN MQW structure was regrown in a *Mn-free reactor.* After the growth chamber was exposed to air for 12 h, and the graphite susceptor was baked in H_2 ambient at 1100 °C for 1 h. The air-exposed chamber and the H_2-baked susceptor were denoted as the Mn-free reactor. Sample D had a structure and regrowth procedure similar to that of sample C, but it had a Mn-doped GaN underlying layer, as shown in Fig. 1(d). In sample D, up-converter devices were grown with multiple regrowth steps to clarify the effect of Mn contamination in GaN. To study the issue of surface segregation and/or diffusion effect on Mn-doped GaN epitaxy, Mn-doped GaN layers were regrown on *n-GaN templates*, denoted as *Mn-GaN templates*. Sample E with n-GaN (~2 µm) layer was regrown on the *Mn-GaN templates* in a Mn-free reactor [Fig. 1(e)]. As shown in Fig. 1(f), sample F had a layer structure and regrowth procedure similar to those of sample E, but hydrogen chloride (HCl)-etched surface treatment was carried out on the *Mn-GaN templates* for 10 min prior to the regrowth of the n-GaN layer. In the current study, up-converted photoluminescence (UPL) measurements were performed at 12 K to evaluate the optical properties of the samples. The excitation source was He-Cd laser at 325 nm or Ar laser at 488 nm. The UPL signal was dispersed by a monochromator (Acton SP-500) and was detected by a thermoelectrically cooled photomultiplier tube (Hamamatsu R94302) using the photon counting method. Secondary ion mass spectroscopy (SIMS) measurements were carried out to analyze the dopant profiles and redistribution sites in the growth interfaces of Mn. The measurements were performed using the time-of-flight SIMS (CAMECA ims 4f and ION-TOF Secondary Ion Mass Spectrometer, Germany) with O_2^+ sputtering ion source.

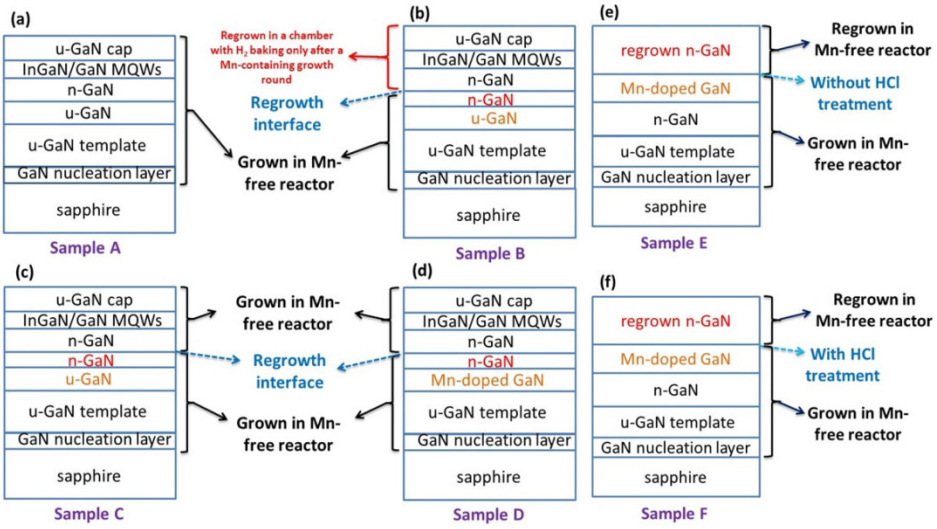

Fig. 1. (a)-(d) Schematic structures in cross-section view for the samples A, B, C and D regrown with varied chamber treatments, respectively. (e)-(f) Schematic structures in cross-section view for the samples E and F grown on Mn-doped GaN templates without and with HCl surface treatments, respectively.

#164357 - $15.00 USD Received 7 Mar 2012; revised 22 Mar 2012; accepted 22 Mar 2012; published 26 Mar 2012

3. Results and discussions

Figure 2(a) shows the typical PL spectra of samples A and B at 12 K excited by a He-Cd laser (325 nm; E_{exc} = 3.51 eV). The spectra taken from samples A and B had strong emission peaks at around 412 and 406 nm, respectively, originating from the InGaN quantum wells (QWs). The weaker peak at around 418 nm of samples B was likely caused by the In fluctuation in the InGaN QWs. The In fluctuation was likely due to the fluctuation of the growth temperature in the growth process. The wavelength difference of the main peak between samples A and B was likely attributed to the diffusion and/or re-incorporation of residual Mn into the InGaN QWs to cause the competition effect between Mn and In atoms during the growth of InGaN material. The details about the competition effect between Mn and In atoms in InGaN alloys will be published elsewhere. Figure 2(b) shows the typical PL spectra of samples A and B excited by an Ar laser (488 nm; E_{exc} = 2.54 eV). No emission peak was observed from sample A because of the excitation photons with energies lower than the band gap of the InGaN QWs. However, an emission peak at around 406 nm (3.05 eV) was observed in sample B. This result is similar to our previous report in that a Mn-doped GaN layer embedded under the InGaN QWs can lead to a linear up-conversion emission [10]. In principle, this result is unreasonable because sample B did not contain any intentionally added Mn-doped layer. To clarify whether the up-conversion emission from the sample B caused by the residual Mn contamination in the MOCVD reactor (memory effect), SIMS was performed to evaluate the Mn incorporation and redistribution behavior in the regrowth junction layers of sample B.

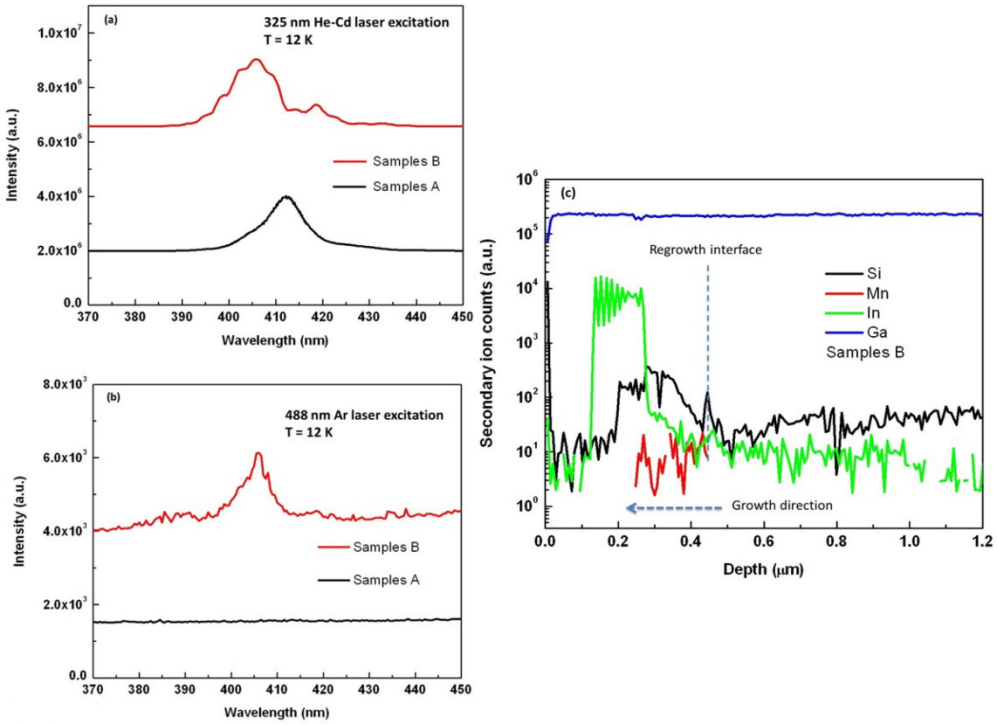

Fig. 2. Low temperature (12 K) PL spectra of samples A and B excited by (a) 325 nm He-Cd laser and (b) 488 nm Ar laser (c) SIMS profiles of Ga, In, Mn and Si elements taken from the sample B as a function of depth from the surface.

Figure 2(c) shows the profiles of Ga, In, Mn and Si elements taken from sample B as a function of depth from the surface, giving evidence that Mn atoms remained in the MOCVD reactor after a round of Mn-containing growth. Note that spike-like profiles of the Ga, In, and Si elements on the surface of sample B can be attributed to the artifacts and surface effect of

#164357 - $15.00 USD Received 7 Mar 2012; revised 22 Mar 2012; accepted 22 Mar 2012; published 26 Mar 2012

SIMS measurements, and the Si signal spike at the regrowth interface is most likely caused by some artifacts and the defect-enhanced gettering effect at the imperfect interface during regrowth. In the case of Mg doping in GaN grown by MOCVD, H_2-ambient thermal backing for the reactor and wafer susceptor is a simple method that eliminates the memory effect of Mg dopants between sequent growth rounds. Although the MOCVD chamber with bare graphite susceptor was baked in H_2 ambient at 1100 °C for 1 h before the growth of sample B, which was expected to remove the residual Mn atoms on the reactor walls (i.e., to reduce the Mn memory effect) and the susceptor, the detectable Mn background signal was observed, as shown in Fig. 2(c). This effect can be attributed to Mn contamination in the reactor and clearly indicating the presence of the Mn doping memory effect corresponding to the anomalous up-conversion signal from sample B without Mn-doped GaN detection layer [10]. Thus, the memory effect cannot be effectively eliminated by the H_2-baking method.

To eliminate the Mn memory effect after Mn-containing growth procedures were conducted in the MOCVD chamber and graphite susceptor, the chamber and susceptor were exposed to air first and sequentially baked in H_2 ambient at 1100 °C. Next, samples C and D were grown in this MOCVD reactor. Figure 3(a) shows the typical PL spectra of samples A, C, and D at 12 K excited by a He-Cd laser (325 nm). These spectra taken from samples A, C, and D had strong emission peaks at around 412, 417, and 406 nm, respectively. Peaks at the long wavelength side of the PL spectra taken from samples C and D were likely caused by the In fluctuation in the InGaN QWs. On the other hands, the difference between the sample A and the sample C was likely attributed to the fluctuation of the round-to-round stability of growth temperature in the growth process. The difference in dominant peak wavelengths between samples C and D can be attributed to the same origin, such as samples A and B.

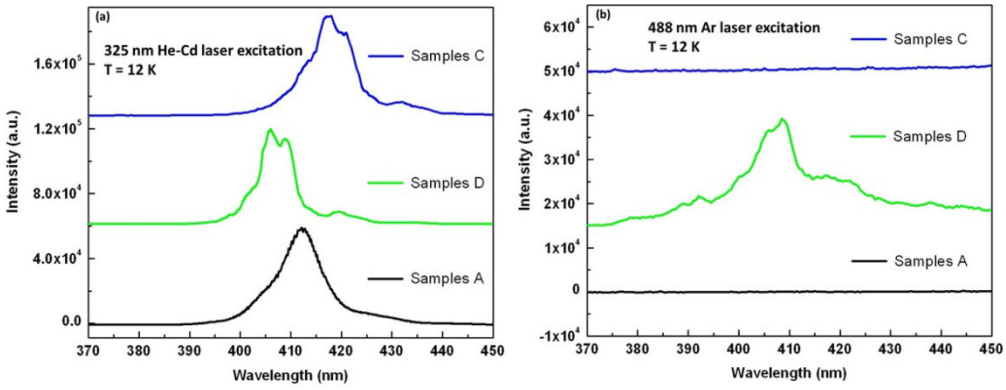

Fig. 3. Low temperature (12 K) PL spectra of samples A, C and D excited by (a) 325 nm He-Cd laser (b) 488 nm Ar laser.

Figure 3(b) shows the typical PL spectra of samples A, C, and D excited by an Ar laser (488 nm; E_{exc} = 2.54 eV). A strong emission peak at around 406 nm was observed from sample D. This up-conversion PL (UCPL) emission and related mechanisms have been described in our previous report [10]. As expect, no UCPL emission peak was observed from samples A and C. These results imply that the anomalous UCPL emission observed in sample B associated with the memory effect of Mn dopants can be suppressed by exposing the chamber to air and sequentially backing the graphite susceptor in H_2 ambient. SIMS measurements were performed to evaluate the Mn incorporation in sample C, clarifying further whether the disappearance of the anomalous UCPL emission from sample C was caused by the elimination of Mn memory effect through air-exposed and H_2-backing treatments. Figure 4(a) shows the Ga, In, Mn, and Si dopant profiles as a function of depth from the surface of sample C. Clearly, Mn atoms were not detected in this sample because the signal level of Mn atoms was well below the detection limit. These results indicate that the

#164357 - $15.00 USD Received 7 Mar 2012; revised 22 Mar 2012; accepted 22 Mar 2012; published 26 Mar 2012

memory effect of Mn due to the residual Mn contamination in MOCVD reactor can indeed be eliminated by air-exposed and H_2-baking treatments before the growth of sample C, making the unexpected UCPL emission absent, as shown in Fig. 3(b). The mechanism of residual Mn dopants removed by air-exposed and H_2-baking treatments can be tentatively attributed to the fact that the residual Mn atoms in the reactor walls and graphite susceptor are first oxidized to form the Mn-O complexes. These Mn-O complexes are then removed from the reactor and are desorbed from the susceptor by the slipstream of H_2 carrier gas at a high temperature of 1100 °C. Figure 4(b) plots the Ga, In, Mn, and Si dopant profiles from sample D as a function of depth from the surface taken from SIMS measurement. The asymmetrical switch-on and -off profiles of Mn dopants may be caused by the memory effect, surface segregation, and/or diffusion associated with the re-incorporation from the reactor and/or redistribution of Mn atoms in the Mn-containing epitaxial layer. In the case of the memory effect, Mn precursor adsorbed onto the reactor walls and graphite susceptor during the growth of Mn-doped GaN layer.

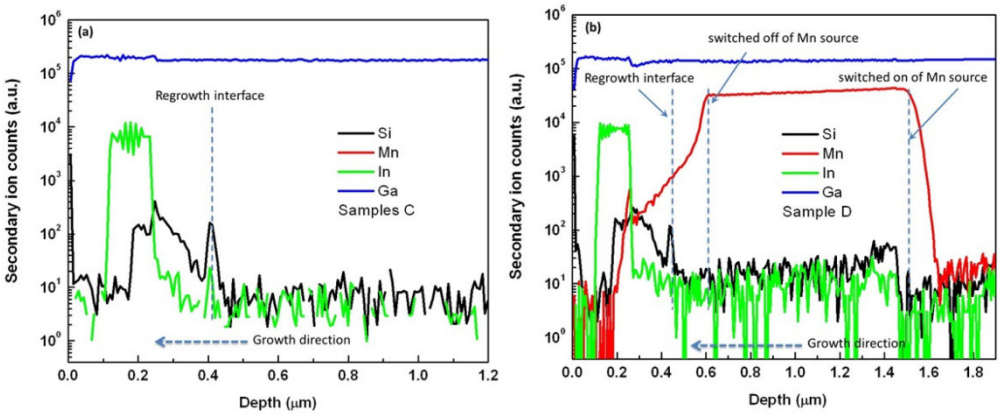

Fig. 4. SIMS profiles of Ga, In, Mn and Si elements taken from the (a) sample C and (b) sample D.

The Mn-related residuals were released as a gas phase, even when the Mn source line was switched off, causing the continuing re-incorporation of Mn into the unintentionally Mn-doped layers. In the case of surface segregation and diffusion, a layer of Mn-rich material developed on the growing surface, which became the source of Mn diffusion for the observed slow-decay Mn tail extending to the subsequent growth layers after the Mn source line was switched off. Again, note that the air-exposed and H_2-baking treatments were performed before the growth of sample D. Thus, the Mn memory effect was assumed eliminated. The long Mn tail after regrowth of unintentionally Mn-doped layers in the sample D could have originated from a Mn-rich (e.g., surface segregation) surface layer or the Mn-doped GaN underlying layer itself. If a Mn-rich surface layer existed on the surface of a Mn-doped GaN layer, the re-incorporation of Mn into the sequential unintentionally Mn-doped layer could take place through re-evaporation into the gas phase and thereby incorporating into the regrowth layers from the gas phase. In the case of the long Mn tail in the unintentionally Mn-doped GaN overgrown layer, the regrowth step involving a high-temperature process could lead to the redistribution of Mn from the Mn-doped GaN underlying layer diffusion along the growth direction to the subsequent overgrown layers.

#164357 - $15.00 USD Received 7 Mar 2012; revised 22 Mar 2012; accepted 22 Mar 2012; published 26 Mar 2012

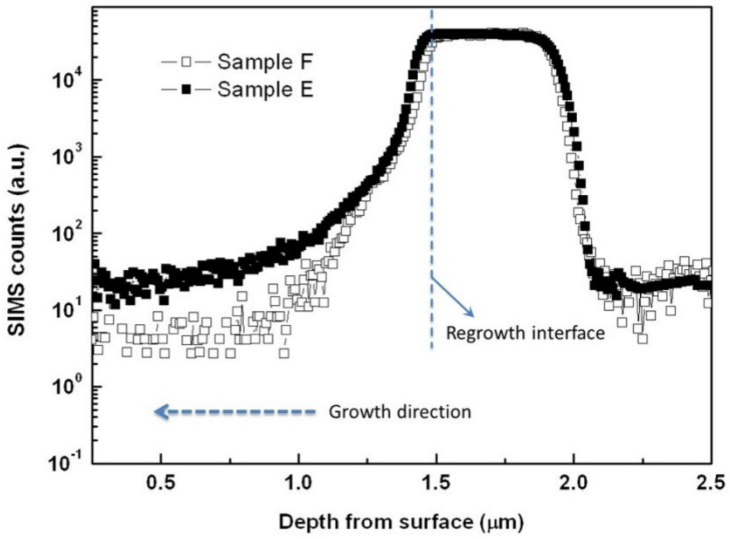

Fig. 5. SIMS profiles of Mn element taken from the samples E and F.

To clarify further the issue of Mn surface segregation as well as the diffusion in GaN and redistribution at the regrowth interface, samples E and F were also prepared. To identify whether the accumulation of Mn on the surface of *Mn-GaN templates* occurred, some of the *Mn-GaN templates* were treated in HCl solution for 10 min prior to the loading of wafers into the reactor. After the HCl-treatment procedure, the Si-doped n-GaN layer was regrown on the *Mn-GaN templates,* and the wafers were labeled as sample F. Other wafers grown on the *Mn-GaN templates without the* HCl-treatment procedure were labeled as sample E. Figure 5 shows the SIMS measurements of the Mn dopant profiles from sample E as a function of depth from the surface. Clearly, the Mn profile referring to the switch-on and -off points of the Mn precursor was markedly asymmetrical. This result is similar to that in sample D, as shown in Fig. 4(b), which is caused by the memory effect, surface segregation, and diffusion associated with the re-incorporation and redistribution of Mn atoms. The Mn profile of sample E exhibited a significant long tail extending to the sequentially regrown n-GaN layer. Compared with that of sample D, the Mn profile of sample E indicates that the Mn profile with long-tail behavior in regrown n-GaN layer is different from the diffusion behavior of Mn in the InGaN layer of sample D, as shown in Figs. 4(b) and 5. Figure 5 also shows the SIMS measurements of the Mn dopant profiles as a function of depth from the surface of sample F. The signal intensity of Mn near the surface of sample F was lower than that of sample E without the HCl treatment process performed on the *Mn-GaN templates*. In other words, the segregation of Mn or Mn-rich complexes may indeed exist near the surface of *Mn-GaN templates*, and they can be partially removed by dipping in HCl solution. In addition to the effect of the contamination from the Mn in the QWs, it was also important to refer to the other factors that lead to limitation in the optical properties and/or internal quantum efficiency for InGaN QWs, specifically the charge separation effect. The charge separation from the polarization fields in the QW would lead to reduction of the electron-hole wavefunction overlap and radiative recombination rate in particular for green-emitting QWs. Recently, some approaches to address this issue have been reported by using InGaN QWs with large overlap design [33,34] or semi/nonpolar InGaN QWs [35,36]. In the case of large overlap design, staggered InGaN QWs with large electron-hole wavefunction overlap and improved radiative recombination rate as well as internal quantum efficiency were investigated for nitride LEDs application. In the case of semi/nonpolar InGaN QWs, the AlGaN-cladding-free m-plane

#164357 - $15.00 USD Received 7 Mar 2012; revised 22 Mar 2012; accepted 22 Mar 2012; published 26 Mar 2012

InGaN/GaN laser diodes with threshold current densities that were comparable to state-of-the-art c-plane InGaN/GaN laser diodes were demonstrated.

4. Conclusions

In summary, the current study revealed the Mn memory effect of the MOCVD reactor. Redistribution of the Mn dopants during subsequent regrowth layers in a Mn-free MOCVD chamber was also observed. In addition to the memory effect, the high residual Mn level and the slow decay rate of the Mn concentration tail could be also attributed to the surface segregation and redistribution of Mn from the Mn-doped GaN underlying layer. The contamination effect of the residual Mn in the reactor could be eliminated effectively by the air-exposed and H_2-baking procedure. Comparing the Mn profiles from the samples grown on Mn-GaN templates with different surface treatments, the segregation of Mn at Mn-doped GaN surface was also reasonably speculated to lead to the Mn dopant tail in the regrown undoped GaN layers.

Acknowledgments

Financial support from the Bureau of Energy, Ministry of Economic Affairs of Taiwan, ROC, through grant No. 100-D0204-6 and the LED Lighting Research Center of NCKU are appreciated. The authors would also like to acknowledge the National Science Council for the financial support of the research Grant Nos. NSC 98-2221-E-218-005-MY3, 100-2112-M-006-011-MY3 and 100-3113-E-006-015.

#164357 - $15.00 USD Received 7 Mar 2012; revised 22 Mar 2012; accepted 22 Mar 2012; published 26 Mar 2012